J. Membrane Biol. 183, 125–135 (2001)
DOI: 10.1007/s00232-001-0060-y

The Journal of
Membrane
Biology

Sizing the Radius of the Pore Formed in Erythrocytes and Lipid Vesicles by the Toxin Sticholysin I from the Sea Anemone *Stichodactyla helianthus*

M. Tejuca[1,2], M. Dalla Serra[1], C. Potrich[1], C. Alvarez[2], G. Menestrina[1]
[1]CNR-ITC, Centro di Fisica degli Stati Aggregati, I-38050 Povo (Trento), Italy
[2]Departamento de Bioquimica, Universidad de la Habana, La Habana, Cuba

Received: 29 November 2000/Revised: 31 May 2001

Abstract. The radius of the pore formed by sticholysin I and II (StI, StII) in erythrocytes and sticholysin I in lipid vesicles was investigated. The rate of colloid osmotic lysis of human erythrocytes, exposed to one of the toxins in the presence of sugars of different size, was measured. The relative permeability of each sugar was derived and the pore radius estimated with the Renkin equation. The radius was similar for sticholysin I and II and was independent of the reference sugar chosen and of the toxin concentration applied. It was also the same when erythrocytes were pretreated with different toxin doses in the presence of a polyethylene glycol (PEG) large enough to prevent lysis and thereafter transferred to solutions containing oligosaccharides of different size where they did lyse at different rates. The osmometric behavior of large unilamellar vesicles (LUV) was thereafter used to estimate the toxin lesion radius in a model system. LUV transferred to a hyperosmotic solution with a certain sugar immediately shrank and then re-swelled at a rate dependent on the bilayer permeability to water and sugar. When LUV were previously permeabilized with StI, only a fraction of them, namely those not carrying pores, continued to behave as osmometers. By increasing the size of the added sugar and approaching the pore radius, the fraction of osmometric LUV increased. Relative permeabilities were derived and used to estimate a channel radius around 1.2 nm, both for sugars and for PEGs. In conclusion the sticholysin pore has a constant size independent of toxin concentration and similar in natural and artificial membranes, suggesting it has a fixed predominant structure.

Key words: Colloid-osmotic lysis — Erythrocytes — Large unilamellar vesicles — Osmotic jump — Light scattering — Stopped flow — Actinoporin

Correspondence to: G. Menestrina
menes@cefsa.itc.it

Introduction

Sticholysin I (StI) and II (StII) are basic cytolysins purified from the Caribbean sea anemone *Stichodactyla helianthus.* They belong to a group of highly homologous proteins, characterized by high pI, molecular size around 20 kDa, inhibition by sphingomyelin [1, 12, 24, 34] and predominant beta structure [6, 40], which are collectively called actinoporins [24].

Most, maybe all, actinoporins are capable of forming oligomeric pores in cell and lipid membranes [1, 12, 24, 34], therefore belonging to the pore-forming toxins (PFT) family. Studying actinoporins is important not only to understand their envenoming properties, but also, and more in general, to investigate basic mechanisms such as: polypeptide insertion into membranes, self aggregation, pore assembly and solute permeation through the newly formed pores [28, 32]. In addition, they have the potential of becoming tools for biotechnological and pharmaceutical applications. In fact, they have already been used for the construction of antitumoral and antiparasite chimeric molecules [7, 8, 47, 57]. In this respect, eukaryotic actinoporins are an interesting alternative to the most frequently used bacterial toxins [26, 52].

Studies on the structure and function of actinoporins have made major advances with equinatoxin II, from *Actinia equina*, after its cloning and expression in a bacterial system [2], which allowed site-directed mutagenesis. A cystein-scanning study [4, 5] has individuated 3 regions of possible insertion into the lipid layer, the N-terminus, containing a highly conserved amphiphilic helix, a central domain containing a cluster of aromatic residues, and 2 residues in the C-terminal part of the

molecule. That the three tryptophans of the central cluster are quickly transferred into the lipid phase has been confirmed by direct mutations of these residues [37]. Similarly, the important role of the N-terminus has been indicated also by truncation experiments [3]. Given the high degree of homology which is present in the group, these features are likely to be representative also for all other actinoporins. The three-dimensional structure of soluble equinatoxin II has now been completely solved by X-ray crystallography [6].

While it is clear that StI and StII exert their cytolytic action by forming oligomeric pores in the cell membrane [1, 56] due to the instability of these oligomers, their stoichiometry is not well established yet. Most evidence suggests, for these and other actinoporins, that a tetramer is the preferred structure [10, 38], however, it is still not clear whether only one oligomeric form exists, or whether pores can have different sizes and the tetramer is only the average result.

In this work we have tried to establish if the structure of the sticholysin pore is fixed or not, by measuring its hydrodynamic radius both in red blood cells and in purely lipidic vesicles as a function of toxin concentration. If different forms in fact, exist, larger pores would be expected at higher toxin doses. While the estimate of pore radius in red blood cells, based on their colloid-osmotic properties, is an established technique, that with vesicles is not trivial due to their small volume. In fact, osmotic shrinkage/swelling of these tiny objects is very quick and requires a stopped-flow approach suitable for resolving fast kinetics [16].

Materials and Methods

Toxins and Reagents

StI and StII were purified according to a described procedure [30], combining gel filtration chromatography on Sephadex G-50 medium (Amersham-Pharmacia Biotech, Upsalla, Sweden) and Ionic Exchange Chromatography on CM-cellulose 52 (Whatman, Kent, UK). StI has the same N-terminus sequence as the toxin previously called C I by Kem and Dunn [25], whereas StII corresponds to the cytolysin C III isolated by Blumenthal and Kem [15].

Calcein was obtained through Sigma and Triton X-100 from Merck (Darmstadt, Germany). Lipids used were egg phosphatidylcholine (PC) and sphingomyelin (SM) both from Avanti Polar Lipids (Alabaster, AL), and were more than 99% pure according to the purchaser. Glycerol, ethylene glycol, glucose, sucrose, raffinose, maltohexaose, maltoheptaose were from Sigma (Milan, Italy), stachiose and maltopentaose were from Acros Organics (Geel, Belgium) and all PEGs (PEG200, PEG300, PEG400, PEG600, PEG900, PEG1000, PEG2000 and PEG3000) were from Fluka (Buchs, Switzerland).

Lysis of Red Blood Cells

Hemolysis was assayed by measuring the decrease in turbidity of a human red blood cell suspension at 650 nm with a microplate reader (UVmax, Molecular Devices, Sunnyvale, CA), as already described [47, 57]. Human red blood cells (HRBC) were prepared from total blood obtained intravenously from healthy volunteers, by washing thrice (10 min centrifugation at 700 × g, room temperature) in 10 mM Tris-HCl, 140 mM NaCl, pH 7.4 (TBS). In each well, a fixed concentration of StI was present, in a final volume of 100 μl of TBS, with or without 30 mM of one oligosaccharide or PEG (as specified in the text). The reaction was started by adding 100 μl of HRBC (preequilibrated with the same osmoticant), at a titre corresponding to an initial A_{650} value of around 0.1. The microplate was shaken and read every 8 sec for the first 30 or 45 min and thereafter at a lower frequency for up to 2 hr 30 min.

Alternatively, HRBC were permeabilized using different toxin concentrations in the presence of PEG 3000, which is big enough to prevent hemolysis but allows pore formation. Such permeabilized HRBC were then separated from unbound toxin by repeated centrifugation, always in the presence of PEG 3000. Finally, 20 μl of permeabilized HRBC were transferred to the wells of a microplate and supplemented (at time zero) with 180 μl of TBS buffer containing or not 30 mM of the different oligosaccharides. The plate was then kinetically read as above. Also in this case HRBC counts were chosen such that initial A_{650} values were around 0.1.

Due to the peculiar osmotic properties of larger PEGs (e.g., PEG2000 and PEG3000 [48]), in some experiments (as specified in the text) instead of being used at a constant 30 mM concentration, like the oligosaccharides, they were added at a constant osmolarity of 60 mOsm, which corresponds approximately to the measured osmolarity of 30 mM PEG2000 [48]. The osmolarity of the various solutions was measured with a cryoscopic osmometer (Osmomat 030, Gonotec, Berlin, Germany).

The colloid-osmotic hemolysis hypothesis is based on the different permeability of a damaged erythrocyte membrane for bulk osmoticants of different size. Along an outward osmotic gradient of nonpermeant molecules (such as hemoglobin), net influx of water increases cell volume until the cell membrane breaks [36]. Such an effect can be prevented by addition to the incubation medium of an osmotic protectant of appropriate size that is too large to enter the cell through the pores and therefore counterbalances the increased intracellular pressure. In the case of StI and StII, addition of large osmoticants, indeed, increased the time $t_{1/2}$ necessary to reach 50% of hemolysis, in a size-dependent way (*see* Fig. 1*A*). We used $t_{1/2}{}^{s} - t_{1/2}{}^{0}$, ($t_{1/2}{}^{s}$ and $t_{1/2}{}^{0}$ being the half-time with or without the osmolites respectively) as an estimate of the delay introduced by the osmotic protectant, which in turn represents the time necessary for it to diffuse inside the cell through the toxin-induced lesions. According to [21], $1/(t_{1/2}{}^{s} - t_{1/2}{}^{0})$ is related to the permeability p_s of the sugar *s* through the cell membrane by:

$$1/(t_{1/2}{}^{s} - t_{1/2}{}^{0}) = p_s \cdot A/V \tag{1}$$

where A and V are average area and volume of the cell. Provided that the spontaneous permeability of the osmolite through the RBC membrane is small enough in comparison to that mediated by the toxin-induced pores (which generally is true, as we will see), and assuming that for a given toxin concentration an average of n pores are formed per each RBC, we can write:

$$p_s \cdot A = n P_s \tag{2}$$

where P_s is the single pore permeability of the osmolite *s*.

The Renkin equation [22, 49] provides a link between the permeability P_s of an uncharged molecule of radius x and that of a reference molecule of radius a(P_a) through a noninteracting pore of radius *r:*

$$P_s/P_a = \frac{(1 - A \cdot (x/r) + B \cdot (x/r)^3 - C \cdot (x/r)^5) \cdot (1 - x/r)^2}{(1 - A \cdot (a/r) + B \cdot (a/r)^3 - C \cdot (a/r)^5) \cdot (1 - a/r)^2} \tag{3}$$

where *A*, *B* and *C* are three numerical coefficients (2.104, 2.09 and 0.95, respectively). Provided that we compare data obtained with cells of the same average area and volume and at the same toxin concentration (i.e., same *n*), the observed delays can be used, through Eq. *1* and *2*, to build a Renkin plot relating the relative permeability of the molecule with its size via Eq. *3*.

Preparation of Lipid Vesicles

Large unilamellar vesicles (LUV200) were prepared by extrusion of a solution containing freeze-thawed multilamellar liposomes [33, 39] in a buffer containing or not 40 mM or 80 mM calcein (m.w. 710) and enough NaOH to give pH 7.0. The lipid used was a 1:1 mixture of PC and SM always at a starting lipid concentration of 5 mg/ml. Extrusion was performed by 31 passages in a LiposoFast Basic Unit of Avestin Inc. (Ottawa, Canada) equipped with two stacked polycarbonate filters bearing holes with an average diameter of 200 nm (Nuclepore, Maidstone, UK). Direct measurement of LUV size was performed by photon correlation spectroscopy (as in [39], using a laser particle sizer (Malvern Z-sizer 3, Malvern, UK) and lead to a diameter of 180 ± 10 nm. To remove untrapped calcein, LUVs were spun through minicolumns loaded with Sephadex G50-medium (Amersham-Pharmacia) according to [31], and pre-equilibrated with a buffer containing 10 mM HEPES, 100 mM NaCl, 1 mM EDTA pH 8 (buffer *A*) or 10 mM HEPES, 1 mM EDTA pH 8 (buffer *B*).

Osmotic-Jump Experiments with Intact Vesicles

A two-syringe stopped-flow spectrometer (model SF-51, Hi-Tech Scientific, Salisbury, UK), interfaced to a personal computer, was used in the fluorescence configuration [19]. Typically, one syringe contained vesicles (loaded with 40 mM calcein) in buffer *A* at a lipid concentration of 50 μg/ml (63 μM, assuming an average lipid molecular weight of 800 D). The other syringe contained a hyperosmotic solution prepared by adding to the same buffer either glucose or glycerol at a constant osmolarity of 1.6 Osm. An equal amount from each syringe was pneumatically injected through the mixer into the observation cell with a measured dead time, between mixer and cell, of around 7 milliseconds. The injecting syringes, the mixing chamber and the observation cell were all thermostatted to 25°C by a water circulation bath. The time course of the light emitted at 90° was followed after the trigger signal from the stop syringe [19]. Either calcein fluorescence emission or vesicle light scattering were recorded. For calcein signal, excitation was set at 485 nm by a monochromator, and emission was high-pass filtered at ≥530 nm with an optical filter (Schott OG530). This allowed an estimate of calcein self-quenching. To measure the light-scattering instead, excitation was selected at 360 nm and no filter was used in emission. An increase of calcein signal indicated vesicle swelling, which is accompanied by a decreased self-quenching of calcein [17, 29]. Conversely, an increase of light-scattering indicated vesicle shrinkage, which causes an increase of the form-factor [16, 50].

Osmotic-Jump Experiments with Permeabilized Vesicles

For these experiments calcein-free LUV were prepared in buffer *B*. When pre-permeabilized, these LUV were incubated at 50 μg/ml (63 μM), in buffer *B* (30 min, room temperature) with an StI dose calculated to produce either 50% or 80% of release. The required dose was 2.4 μg/ml (0.12 μM) and 6 μg/ml (0.3 μM), respectively, as determined in parallel experiments performed using LUV loaded with 80 mM calcein as described earlier [56]. Briefly, the fluorescence of released calcein was measured with a spectrofluorimeter (FP550, Jasco, Cremalla, Italy) exciting at 494 nm and detecting at 520 nm. To a cuvette containing 50 μg/ml (63 μM) of LUV in buffer *B*, various amounts of StI were added and the percentage of release, R, was calculated as:

$$R_{\%} = (F_{\text{fin}} - F_{\text{in}})/(F_{\text{max}} - F_{\text{in}}) \cdot 100 \quad (4)$$

where F_{in} and F_{fin} represent the steady-state values of fluorescence before and after toxin addition, and the maximum release, F_{max}, was obtained with 1 mM Triton X-100. The concentrations inducing 50% or 80% release were extrapolated from the observed dose dependence of $R_{\%}$. The rationale for choosing such values of $R_{\%}$ is that, assuming a Poisson distribution of pores on the vesicles, the following relation holds between R and ν, the average number of pores present on the vesicles [54]:

$$\nu = -\ln (1 - R_{\%}/100) \quad (5)$$

Therefore, the chosen conditions of $R_{\%} = 50\%$ and 80%, would correspond to having $\nu = 0.7$ and $\nu = 1.6$ respectively. This means that each permeabilized vesicle should contain approximately 1 pore in the first case, and 2 pores in the second. Osmotic-jump experiments were performed as above except that buffer *B* was used and the hyperosmotic solution contained 0.56 Osm of different oligosaccharides or PEGs (as specified in the text). Control experiments were performed with intact LUVs.

Abbreviations

StI, *Stichodactyla helianthus* sticholysin I; StII, sticholysin II; SM, sphingomyelin; PC, phosphatidylcholine; EG, ethylene glycol; PEG, polyethylene glycol; Triton X-100, octylphenoxy polyethoxy ethanol; HRBC, human red blood cells.

Results and Discussion

Hydrodynamic Radius of the StI and StII Pores in Red Blood Cells

An estimate of the size of the pore formed by StI in red blood cells was obtained by taking advantage of the colloid-osmotic characteristic of hemolysis induced by this toxin. Using human erythrocytes, we determined the rate of hemolysis in the presence or not of oligosaccharides of different size, all at a concentration of 30 mM (Fig. 1*A*). An estimate of the relative permeability of each oligosaccharide was derived from the inverse of the delay that it introduced in the hemolysis curve with respect to the control (saline buffer only). Such permeability was found to be inversely related to oligosaccharide size. The following oligosaccharides were used (in parenthesis, their hydrated radii as reported in [27, 53]): glucose (0.42 nm); sucrose (0.54 nm); raffinose (0.66 nm); stachiose (0.76 nm); maltopentaose (0.82 nm); maltohexaose (0.90 nm); maltoheptaose (0.98 nm).

Dividing the data of Fig. 1*A* by the permeability of a reference oligosaccharide, they could be arranged in a Renkin plot [22, 49], which provided an estimate of the

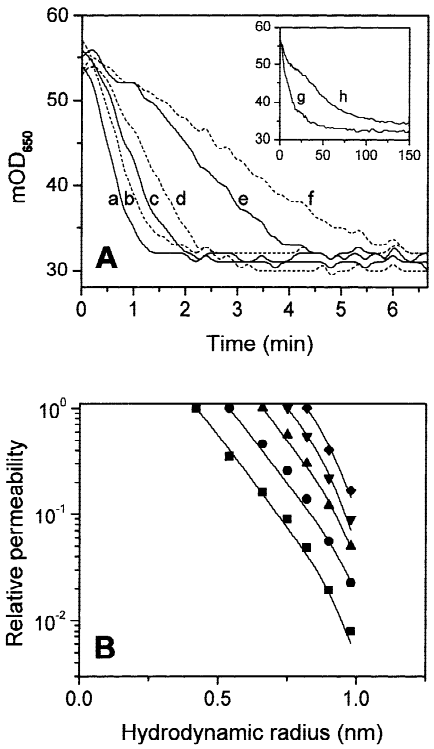

Fig. 1. Colloid osmotic properties of hemolysis induced by StI. (*A*) The rate of toxin-induced hemolysis of human erythrocytes in TBS was determined by measuring the decrease in turbidity after the addition of 16 ng/ml (0.8 nM) StI. The following oligosaccharides of different size were added, all at 30 mM concentration (the number in parenthesis represents their hydrated radius in nm [53]): a) control (no oligosaccharide); b) glucose (0.42); c) sucrose (0.54); d) raffinose (0.66); e) stachiose (0.76); f) maltopentaose (0.82); g) maltohexaose (0.90); h) maltoheptaose (0.98 nm). (*B*) An estimate of the permeability of each oligosaccharide was derived from the inverse of the delay that it introduced in the hemolysis curve (*see A*) with respect to the control. Relative permeabilities were then obtained by dividing by the permeability of a reference oligosaccharide, and the data were arranged in a Renkin plot providing an estimate of the pore radius. The reference oligosaccharide was either glucose (squares), sucrose (circles), raffinose (upward triangles), stachiose (downward triangles) or maltopentaose (diamonds). Solid lines are best fits of the Renkin equation providing (in the same order as above) a radius of 1.09 ± 0.02, 1.13 ± 0.02, 1.11 ± 0.02, 1.08 ± 0.02 and 1.09 ± 0.02 nm, respectively.

pore radius (Fig. 1*B*). This procedure was repeatedly applied, choosing different oligosaccharides as the reference, and best fit values of the Renkin radius were calculated in each case, as reported in the figure. In this way, we ascertained that the estimated radius (approximately 1.1 nm) does not depend on the oligosaccharide chosen as the reference.

Thereafter, the same approach was used to estimate the pore radius as a function of the concentration of the toxin applied (Fig. 2). In fact, if pores of different size could be formed, one should expect that larger pores, requiring a higher number of constituent monomers, should appear at larger doses of the toxin. To the contrary, and despite the fact that under these conditions the absolute rate of hemolysis varied by orders of magnitude indicating there was no saturation in the amount of toxin bound (Fig. 2*A*), the Renkin plot gave always very similar extrapolated radii (Fig. 2*B*). The best-fit results with the series of oligosaccharides is reported as a function of toxin dose in Fig. 2*C* (squares).

Since very often polyethylene glycols (PEGs) are used in place of oligosaccharides to determine the osmotic properties of ion channels [13, 14, 51, 59], we repeated these experiments using also a series of PEGs (Fig. 2*C*, circles). These were: EG (0.22 nm); PEG200 (0.40 nm); PEG300 (0.48 nm); PEG400 (0.56 nm); PEG600 (0.69 nm); PEG900 (0.85 nm); PEG1000 (0.89 nm); PEG1500 (1.1 nm); PEG2000 (1.27 nm); PEG3000 (1.40 nm), where again, in parenthesis, we state the hydrodynamic radius taken from [27]. Since the osmolarity of PEG solutions increases faster than their concentration (especially with larger molecules like PEG2000 and PEG3000 [48]), experiments were performed either at a constant 30 mM concentration, as with the oligosaccharides (open circles), or at a constant osmolarity of 60 mOsm (filled circles) with practically the same results.

Whereas it is clear that with both oligosaccharides and PEGs, the radius of the pore does not depend on the concentration of the toxin, the estimates obtained with the two kinds of molecules, on the other hand, were slightly different, i.e., 1.09 nm and 0.96 nm, respectively. This might be due, at least in part, to the fact that nonhydrated radii have been used for PEGs, whereas available hydrated values were used for oligosaccharides. A hydration layer of 0.05 to 0.1 nm is indeed a reasonable value [27, 53]. In addition, a slight underestimate could also result from the fact that PEGs, especially larger ones, are polydisperse in size [11]. It is therefore expected that the fraction with molecular weight larger than the average could plug a pore slightly bigger than the PEG nominal radius, thus producing the observed underestimation of pore size. The fact that, despite being polymeric, PEGs behaved in these experiments as hard spherical molecules is consistent with the results obtained by others [41] in careful experiments on the passage of similar PEGs through the pores formed by staphylococcal α-toxin, where researchers reached the same conclusion. On the other hand, the possibility that PEGs, being linear molecules, unfold in solution and get through the pore in an elongated configuration, would have led to a marked overestimate of pore radius instead of the observed underestimate.

We obtained quite similar results also with StII, a slightly more active isotoxin produced by *S. helianthus* (*inserts* in Fig. 2). The concentration-independent pore radius determined with 30 mM PEGs in this case was 1.05 nm, slightly bigger than that of StI, and in agree-

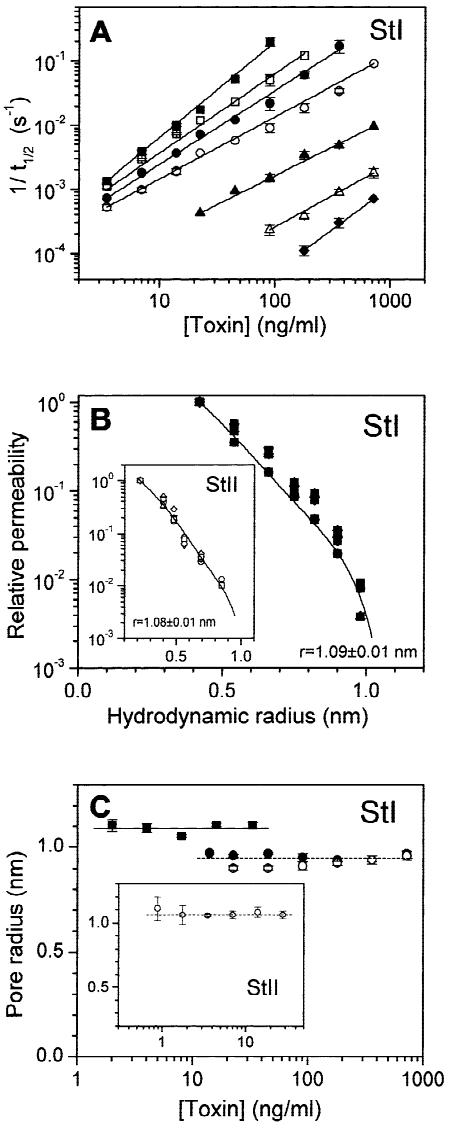

Fig. 2. Dose dependence of the Renkin radius of the pore formed by StI. (*A*) HRBC were exposed to different StI doses in the presence or not of PEGs of different mw. The reciprocal of the time necessary to reach 50% hemolysis ($1/t_{1/2}$) is reported *versus* StI concentration in a double-logarithmic plot. Symbols used are as follows: pure buffer with no PEG (filled squares); PEG200 (open squares); PEG300 (filled circles); PEG400 (open circles); PEG600 filled triangles); PEG900 (open triangles); PEG1000 (filled diamonds). Reported values are averages ± SD of two to four determinations. Straight lines have a slope ranging from 1.0 to 1.5 and indicate that the reaction does not undergo saturation in the concentration interval used. A similar plot for EG was between that for pure buffer and for PEG200 and was not included for clarity. Other conditions as in Fig. 1. (*B*) The approach described in Fig. 1 was used to estimate pore radius as a function of the concentration of the toxin applied. StI was either 32 ng/ml (1.6 nM, squares), 16 ng/ml (0.8 nM, circles), 8 ng/ml (0.4 nM, upward triangles), 4 ng/ml (0.2 nM, downward triangles) or 2 ng/ml (0.1 nM, diamonds). The solid line is the best fit of the Renkin equation to all experimental values providing a radius of 1.09 ± 0.01 nm. In the inset the same kind of experiments done with StII and 30 mM PEGs. StII concentration was either 14 ng/ml (0.7 nM, squares), 7 ng/ml (0.35 nM, circles), 3.5 ng/ml (0.17 nM, upward triangles), 1.8 ng/ml (0.09 nM, downward triangles), or 0.9 ng/ml (0.04 nM, diamonds). PEGs hydrodynamic radii were taken from [27]. The reported dotted line is again the best fit of the Renkin equation to all experimental values, providing radius 1.05 ± 0.01 nm. (*C*) Best-fit values of the Renkin radius of StI, obtained at each toxin dose, are shown either for the series of the oligosaccharides at a constant 30 mM concentration (squares, average ± SD of triplicates), or for that of the PEGs (circles) using either 30 mM constant concentration (open circles, average ± SD of duplicates) or 60 mOsm constant osmolarity (filled circles, average ± SD of triplicates). Other conditions as in Fig. 1. In the inset the same kind of data for StII and 30 mM PEGs (average ± SD of duplicates). Horizontal lines correspond to a radius of 1.09 nm for StI and oligosaccharides, 0.96 nm for StI and PEGs and 1.05 nm for StII and PEGs.

ment with a previously published estimate of around 1 nm [20], which was based on the fact that a dye of molecular weight 795 (acid blue) was permeant through the pore, whereas one of molecular weight 960 (Evans blue) was not. This confirms that different actinoporins, besides a similar primary and secondary structure [3, 9, 30, 40], also have a closely similar mechanism of action.

Since PEG 3000 was able to completely abolish hemolysis, it was used to develop a different approach. HRBC were pretreated with different concentrations of StII in the presence of 30 mM PEG 3000, which prevented hemolysis. Thereafter, they were separated from unbound toxin by washing twice and transferred to a buffer containing or not 30 mM of the various osmoticants. In all cases in which the osmoticant had a size smaller than the radius of the pore, the HRBC started lysing promptly. This is a direct proof that PEG 3000, indeed, prevented lysis by acting as an osmotic protectant and not, for example, by inhibiting toxin binding and/or pore assembly. This approach allowed to estimate directly the rate of HRBC lysis in the presence of the different sugars, without any interference from the kinetics of toxin binding or from transient effects that might occur during toxin absorption and insertion. Even in this case it was possible to observe different rates of lysis with the different oligosaccharides and toxin concentrations (Fig. 3*A*) and the observed half times were again used to build a Renkin plot, similar to those in Figs. 1 and 2. Once more, the derived radius was independent of both the reference sugar and the toxin concentration (Fig. 3*B*). Furthermore, the extrapolated

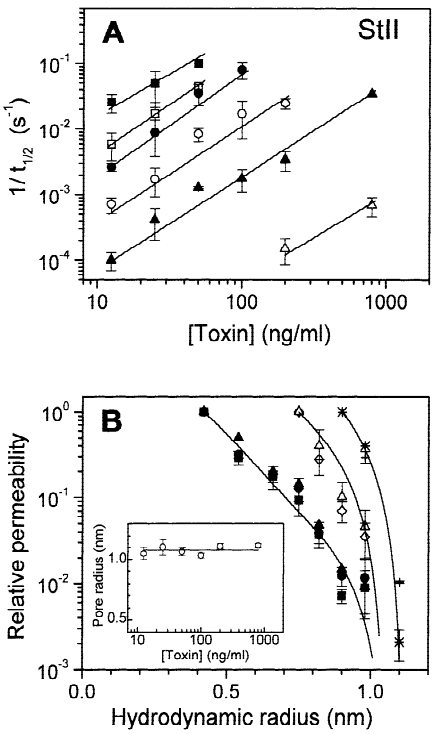

Fig. 3. Estimation of pore radius in HRBC pretreated with StII. (*A*) HRBC pretreated with different doses of StII in the presence of PEG 3000, which prevented hemolysis, were transferred to solutions containing or not 30 mM of different osmolites. The reciprocal of the time necessary to reach 50% hemolysis ($1/t_{1/2}$) was reported *versus* StII concentration as in Fig. 2*A*. Symbols used are as follows: buffer alone (filled squares); sucrose (open squares); raffinose (filled circles); maltopentaose (open circles); maltoheptaose (filled triangles); PEG1500 (open triangles). Reported values are averages ± SD of two to four determinations. Straight lines, with slopes ranging from 1.3 to 1.6, demonstrate that toxin binding had not undergone saturation in the concentration interval used. Plots for glucose, stachiose and maltohexaose were similar and were not included (for clarity). Other conditions as in Figs. 1 and 2. (*B*) The Renkin plot was used to estimate pore radius at the different toxin concentrations used. Applied StII was 12.5 ng/ml (0.6 nM, closed squares), 25 ng/ml (1.25 nM, closed circles), 50 ng/ml (2.5 nM, closed and open triangles), 100 ng/ml (5 nM, open diamonds), 200 ng/ml (10 nM, crosses) or 800 ng/ml (40 nM, asterisks). The reported dashed lines are best fits of the Renkin equation. The derived values of pore radius are shown in the inset as a function of StII dose. The average value, horizontal solid line, is 1.08 ± 0.05 nm.

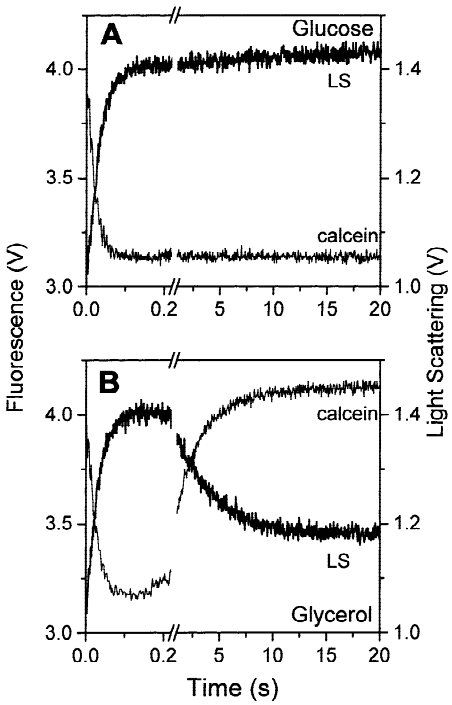

Fig. 4. Osmometric behavior of large unilamellar vesicles. In a stopped-flow photometer with a 90° fluorescence configuration, LUV 200, loaded with 40 mM calcein, were instantly mixed with a hyperosmotic solution and changes in emitted light were recorded. Calcein signal (thin trace, lefthand ordinate) was recorded exciting at $\lambda = 485$ nm and detecting at $\lambda \geq 530$ nm. A decrease of this signal indicates shrinkage of the vesicles (with a consequent increase of calcein self-quenching), whereas an increase indicates swelling. Light-scattering (thick trace, righthand ordinate) was instead measured at $\lambda = 360$ nm with no filter in front of the detector. Because the number and molecular weight of the LUV remained constant, changes in light-scattering were dominated by changes of the form-factor [19, 50]. Henceforth, an increase of this signal indicated shrinkage of the vesicles, whereas a decrease indicated swelling. Two different oligosaccharides were used to establish the osmotic gradient: glucose (panel *A*) or glycerol (panel *B*). Note that in each panel a different time scale was used for the first and the second part of the traces, which were however recorded continuously. Injected solutions were: syringe 1, Buffer *A* with 50 μg/ml (63 μM) LUV; syringe 2, Buffer *A* with 1.6 Osm sugar; mixing was 1:1.

value, 1.08 ± 0.05 nm, was consistent with that estimated before with untreated HRBC.

Characterization of the Osmotic Properties of PC:SM LUV

Having established that the size of the pore formed by StI and StII in red blood cells is constant and independent of toxin concentration, we decided to investigate whether this is true also with lipid bilayer membranes. It is known, in fact, that actinoporins can form pores also in purely lipidic membranes, provided the natural lipid acceptor sphyngomielin is present. Actually, lipid vesicles are a widely used model to investigate the mode of action of actinoporins [2, 10, 20, 35, 57]. Such vesicles are also natural sensors of osmotic pressure [18, 23, 42], and, therefore, they can be used to size the pore formed by StI in experiments conceptually similar to the colloid-osmotic hemolysis.

We began characterizing the osmometric behavior of large unilamellar vesicles (LUV 200) in solution (Fig. 4). LUV containing 40 mM calcein were mixed with an equal volume of a hyperosmotic solution (containing 1.6 Osm of a sugar) and changes in the light emitted at 90°

were followed with a stopped-flow photometer [18, 19, 23]. The oligosaccharide used to establish the osmotic gradient was either glucose (panel *A*) or glycerol (panel *B*). In the early phase, the transient was the same in both cases and indicated a fast shrinkage of the vesicles. This was proven by the decrease of calcein signal, due to an increased self-quenching in the smaller-volume vesicles [17, 29], and by the increase in light-scattering, due to an enhancement of the form-factor [50]. Such shrinkage is rate-limited by the permeability of water through the bilayer [18, 23]. Given the difference in osmolarity between the exterior and interior compartments, the observed transient should correspond to an 80% reduction in the volume of the vesicles. Since their resting volume, *V*, can be calculated as 4×10^6 nm^3, the initial rate of volume change can be estimated, from the traces in Fig. 4, to be $dV/dt\,|_0 = 73 \times 10^6$ nm^3/sec. Such rate of change is related to the bilayer permeability coefficient of water, P_f, by [43]:

$$dV/dt = -A\,P_f v_w\,\Delta c \qquad (6)$$

where *A* is the average surface of one vesicle, v_w the molar volume of water (18 ml/mol) and Δc the outside-inside difference in osmolarity. According to Eq. *6*, and using the pertinent geometric and solution parameters, we could derive the water permeability coefficient for our PC:SM vesicles, which turned out to be 38 μm/sec, in good agreement with published values [17, 29, 43].

In the case of glycerol, shrinking was followed by a slower swelling phase, which was rate-limited by the natural permeability of this oligosaccharide through the membrane [17, 46]. The initial rate of volume change was in that case: $dV/dt\,|_0 = 0.22 \times 10^6$ nm^3/sec. Using again Eq. *6*, and the molar volume of glycerol ($v_g = 73.7$ ml/mol), the bilayer permeability of glycerol resulted in $P_g = 2.8 \times 10^{-2}$ μm/sec, a value comparable to that of 5.4×10^{-2} μm/sec reported earlier for glycerol in membranes of slightly different composition (pure lecithin) and geometry (planar bilayers) [44].

Finally, if glucose was used, the vesicles remained shrunk for the whole duration of the experiment, since this oligosaccharide is practically membrane-impermeant on this time scale [17, 29].

Hydrodynamic Radius of the StI Pore in Lipid Bilayers

Having characterized the osmometric behavior of LUVs, they were used to investigate the properties of incorporated toxin lesions, with the aim of estimating their radius in a model system.

The change in light-scattering due to the initial shrinkage after the osmotic jump was measured with different oligosaccharides or PEGs (the same used for the RBC experiments of Figs. 1 and 2). LUV were either intact (control) or pretreated with known amounts of StI. The results using the PEG series are shown for intact vesicles (Fig. 5*A*) or for LUV permeabilized with an StI concentration, 0.12 μM, suitable to cause the permeabilization of 50% of the vesicles (Fig. 5*B*). This dose was determined in control experiments with calcein-loaded LUV as the concentration that released 50% of the calcein.

Intact vesicles shrank practically at the same rate and to the same extent for all PEGs except for the smaller, membrane-permeant EG and PEG200. The extent of shrinkage of LUV previously permeabilized with StI was instead decreased for all PEGs, but this was more

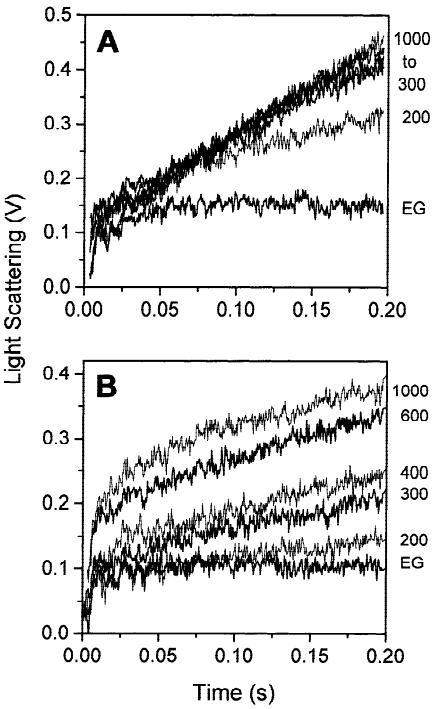

Fig. 5. Osmotic shrinkage of LUV permeabilized or not by StI. The initial change in light-scattering, due to the shrinkage of LUV subjected to an osmotic jump, was measured similarly to Fig. 4 for either intact vesicles (*A*) or for vesicles permeabilized with StI (*B*). Pretreated LUV of (*B*) had been incubated at 50 μg/ml (63 μM) for 30 min with 2.4 μg/ml of StI (0.12 μM), a concentration calculated to cause 50% of permeabilization on the basis of calcein-release experiments. Different PEGs were used: EG; PEG200; PEG300; PEG400; PEG600; PEG1000 (as indicated next to each trace). Injected solutions were: syringe 1, Buffer *B* with 50 μg/ml LUV (63 μM), treated or not with toxin; syringe 2, Buffer *B* with 0.56 Osm sugar; 1:1 mixing. Other experimental conditions as in Fig. 4. Given the reduced outside-inside osmolarity difference, the initial rate of volume change was here lower than in Fig. 4, i.e., $dV/dt\,|_0$ was 22×10^6 nm^3/sec. However, the P_f coefficient of intact vesicles, which could be extrapolated using Eq. 6, was practically the same, i.e., 35 μm/sec. In the case of permeabilized LUV and large osmoticants an early phase of faster shrinkage is seen, which is conceivably due to the higher water permeability through vesicles containing at least one pore.

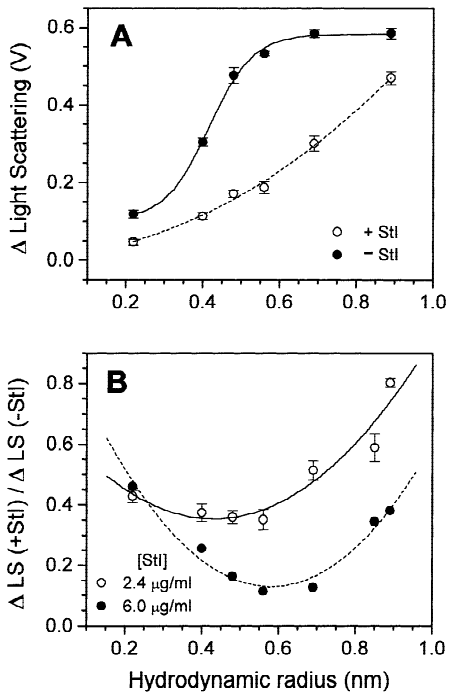

Fig. 6. Extent of osmotic shrinkage of LUV, permeabilized or not by StI, as a function of the size of the osmolite molecule. (*A*) The extent of LUV shrinkage was quantitated by measuring the difference in light scattering between the maximum value induced by the osmotic jump and an initial value taken 2 msec after the stop signal. Different PEGS were used, as shown in Fig. 5. LUVs (63 μM) were either intact (closed circles) or treated with 2.4 μg/ml (0.12 μM) of StI for 30 min (open circles), a concentration that causes 50% permeabilization, as in Fig. 5. Lines drawn have no theoretical meaning. (*B*) The ratio between the extent of shrinkage of vesicles permeabilized or not by StI was calculated for the different PEGs. StI doses sued for the permeabilization were: 2.4 μg/ml (0.12 μM, open circles) or 6 μg/ml (0.3 μM, closed circles) and were meant to cause 50% and 80% release, respectively. Other experimental conditions as in Fig. 5. Lines drawn have no theoretical meaning. The increased ratio observed with the smaller EG was conceivably due to the high spontaneous permeability of this molecule through the membrane itself. This provided a not-negligible, toxin-independent, contribution to the transient, thereby shifting *f* upwards. This effect was not analyzed further.

evident for those of average molecular weight up to 400. This indicates that the permeability of PEGs through the vesicles was increased by StI to a different extent depending on their size.

An estimate of the amount of LUV shrinkage (Fig. 6*A*) was obtained by measuring the difference in light scattering between the maximum value induced by the osmotic jump, as it occurs a few seconds after mixing, and an initial value taken 2 msec after the trigger signal from the stop syringe (a time at which the transient nose coming from the top syringe was finished and the signal was still at a minimum).

Clearly, the extent of shrinkage was in all cases larger with intact LUV than with StI-permeabilized LUV. This was due to the fact that, in the presence of PEGs smaller than the radius of the pore, only the fraction of LUV without StI channels continued to behave as perfect osmometers. LUV with channels were so permeable that they simply didn't change volume. This assumption is justified by the fact that the single-channel permeability of toxin lesions is in general quite large. For example, the single-channel water permeability of the *S. aureus* α-toxin pore was measured to be around 1.5×10^9 nm^3/sec [45]. Since the StI pore is twice as large as the α-toxin pore and probably 1/3 shorter [55, 57], its water permeability can be expected to be approximately 9×10^9 nm^3/sec, which is almost twice that of the whole envelope of one vesicle (i.e., $P_f \times A = 4.8 \times 10^9$ nm^3/sec). This estimate is also in agreement with previously determined permeabilities of non-electrolytes through actinoporin channels. Using radioactive tracers, in fact, Varanda and Finkelstein [58] determined that the single-channel permeability of StII for glycerol was 52×10^6 nm^3/sec, a value which is roughly 15 times that of the whole membrane of one vesicle ($P_g \times A = 3.5 \times 10^6$ nm^3/sec) as determined from Fig. 4.

In the presence of osmoticants so small that their permeation through the pore was faster than our time resolution (approximately 10 msec) the transient light scattering increase due to the shrinkage of LUV with channels was abolished. Therefore, the fraction of non-permeabilized vesicles, f_0, may be estimated from the minimum value of the ratio between the light-scattering increase observed with vesicles permeabilized by StI (called $\Delta LS\,(+StI)$) and that seen with intact LUV (called $\Delta LS\,(-StI)$), as it is detected with a highly permeant solute of permeability P_0 and radius r_0:

$$f_0 = (\Delta LS(+StI)/\Delta LS(-StI))_0 = (\Delta LS(+StI)/\Delta LS(-StI))_{\min} \quad (7)$$

Such minimum was indeed observed with the channel-permeant PEGs of size between 0.4 and 0.6 nm (Fig. 6*B*).

StI doses used in these experiments were chosen, on the basis of control experiments performed with calcein-loaded LUV, to provide either 50% (open circles) or 80% (closed circles) release. Correspondingly, the fraction of intact vesicles, f_0, estimated as in Fig. 6 in a series of 3 independent experiments, averaged, respectively, 49 ± 12% and 18 ± 6% in the two conditions above, very close to the theoretically expected values of 50% and 20% respectively. Using the expression relating the average fraction of permeabilized LUV to the average number of channels per LUV (Eq. 5, originally derived by Schwarz [54]) we calculated that permeabilized vesicles contained on average one pore in the first case, and around two pores in the second case.

On the other hand, when the size of the added PEG approached the radius of the pore, also the permeabilized vesicles started to shrink again because of the reduced

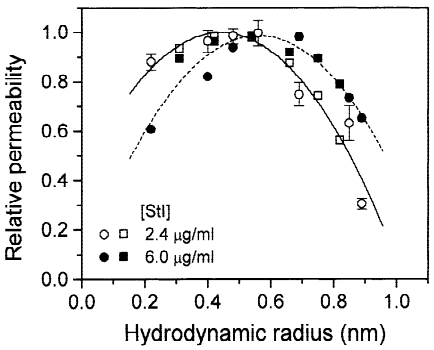

Fig. 7. Relative permeability of different oligosaccharides or PEGS through StI pores as a function of the osmolite size. Relative permeabilities were obtained through Eq. 8 from shrinkage ratios (as those reported in Fig. 6) measured with different oligosaccharides (squares) or PEGs (circles) and after preincubation with different toxin concentrations: 2.4 μg/ml (0.12 μM, open symbols), or 6 μg/ml (0.3 μM, filled symbols). These values suggest a pore radius of at least 1.1 nm in LUV. The parabolic curves through the points do not have a theoretical meaning. Other experimental conditions are as in Figs. 5 and 6.

permeability of these larger molecules through the channel, and the extent of observable shrinkage tended to be restored (Figs. 5 and 6). That the vesicles were indeed permeabilized is indicated also by the increased rate at which water flowed out during the shrinking phase, evidenced by the fast time constant in the light-scattering jump.

The observed light-scattering increase was empirically related to the permeability of the osmoticant by the following relation:

$$(\Delta LS\ (+StI)/\Delta LS\ (-StI))_s = 1 - (P_s/P_0) \cdot (1 - f_0) \quad (8)$$

In fact, in the presence of impermeant sugars $P_s = 0$ and $\Delta LS\ (+StI) = \Delta LS\ (-StI)$, whereas in the presence of very permeant sugars $P_s = P_0$ and $\Delta LS\ (+StI)/\Delta LS\ (-StI) = f_0$, as per Eq. *7*. If such a simple, linear relationship holds, it is possible to derive P_s/P_0 from Eq. 8:

$$P_s/P_0 = (1 - (\Delta LS\ (+StI)\ /\ \Delta LS\ (-StI))_s\ /\ (1 - f_0) \quad (9)$$

Such a ratio is reported in Fig. 7. Application of the Renkin equation to the descending part of the plot, for $r > r_0$, led to an estimate of 1.1 nm, both for oligosaccharides and for PEGs, at an StI concentration of 2.4 μg/ml and around 1.2 nm at 6 μg/ml. It must be noted that the shape of the Renkin curve was not reproducing the experimental points very precisely, thus suggesting that the relationship in Eq. *8* may be oversimplified. Deriving a more realistic expression for Eqs. 8 and 9, however, is outside the scope of this work and will not be attempted.

In conclusion, the size of StI and StII pores seems to be quite constant, around 1.1 nm, and virtually the same in natural and artificial membranes. Either oligosaccharides or PEGs were used for its estimate, however, probably due to their polydispersity, PEGs gave slightly underestimated values. Pore size does not markedly depend on the toxin concentration, suggesting that lesions of constant diameter are formed, both in natural and in model membranes.

This work was financially supported by the Italian Consiglio Nazionale delle Ricerche, by a grant from the Istituto Trentino di Cultura to MT and by a fellowship from the Comune di Trento to CP.

References

1. Alvarez, C., Dalla Serra, M., Potrich, C., Bernhart, I., Tejuca, M., Martinez, D., Pazos, I.F., Lanio, M.E., Menestrina, G. 2001. Effects of lipid composition on membrane permeabilization by Sticholysin I and II, two cytolysins of the sea anemone *Stichodactyla helianthus. Biophys. J.* **80:**2761–2774
2. Anderluh, G., Pungercar, J., Strukelj, B., Macek, P., Gubensek, F. 1996. Cloning, sequencing, and expression of equinatoxin II. *Biochem. Biophys. Res. Commun.* **220:**437–442
3. Anderluh, G., Pungercar, J., Krizaj, I., Strukelj, B., Gubensek, F., Macek, P. 1997. N-Terminal truncation mutagenesis of equinatoxin II, a pore-forming protein from the sea anemone *Actinia equina. Protein Eng.* **10:**751–755
4. Anderluh, G., Barlic, A., Podlesek, Z., Macek, P., Pungercar, J., Gubensek, F., Zecchini, M., Dalla Serra, M., Menestrina, G. 1999. Cysteine scanning mutagenesis of an eucaryotic pore-forming toxin from sea anemone: topology in lipid membranes. *Eur. J. Biochem.* **263:**128–136
5. Anderluh, G., Barlic, A., Potrich, C., Macek, P. Menestrina, G. 2000. Lysine 77 is a key residue in aggregation of equinatoxin II, a pore-forming toxin from sea anemone *Actinia equine. J. Membrane Biol.* **173:**47–55
6. Athanasiadis, A., Anderluh, G., Macek, P. Turk, D. 2001. Crystal structure of the soluble form of equinatoxin II, a pore-forming toxin from the sea anemone *Actinia equina. Structure* **9:**341–346
7. Avila, A.D., de Acosta, M.C., Lage, A. 1988. A new immunotoxin built by linking a hemolytic toxin to a monoclonal antibody specific for immature T lymphocytes. *Int. J. Cancer* **42:**568–571
8. Avila, A.D., de Acosta, M.C., Lage, A. 1989. A carcinoembryonic antigen-directed immunotoxin built by linking a monoclonal antibody to a hemolytic toxin. *Int. J. Cancer* **43:**926–929
9. Belmonte, G. Pederzolli, C., Macek, P., Menestrina, G. 1993. Pore formation by the sea anemone cytolysin equinatoxin II in red blood cells and model lipid membranes. *J. Membrane Biol.* **131:**11–22
10. Belmonte, G., Menestrina, G., Pederzolli, C., Krizaj, I., Gubensek, F., Turk, T., Macek, P. 1994. Primary and secondary structure of a pore-forming toxin from the sea anemone, *Actinia equina* L., and its association with lipid vesicles. *Biochim. Biophys. Acta* **1192:**197–204
11. Berestovskii, G.N., Ternovskii, V.I., Kataev, A.A. 2000. Allowing for polymer polydispersion as a necessary condition for determination of aqueous pore diameters in cell walls and membranes using polymers. *Biofizika* **45:**69–78
12. Bernheimer, A.W. 1990. Cytolytic peptides of sea anemones. *In*: Marine toxins: origin, structure and molecular pharmacology. S. Hall, G. Strichartz, editors. pp. 304–311. American Chemical Society, Washington, DC
13. Bezrukov, S.M., Vodyanoy, I., Parsegian, V.A. 1994. Counting polymers moving through a single ion channel. *Nature* **370:**279–281
14. Bezrukov, S.M., Vodyanoy, I., Brutyan, R.A., Kasianowicz, J.J.

1996. Dynamics and free energy of polymers partitioning into a nanoscale pore. *Macromolecules* **29:**8517–8522
15. Blumenthal, K.M., Kem, W.R. 1983. Primary Structure of *Stoichactis helianthus* cytolysin III. *J. Biol. Chem.* **258:**5574–5581
16. Carroll, J., Ellar, D.J. 1993. An analysis of *Bacillus thuringiensis* delta-endotoxin action on insect-midgut-membrane permeability using a light-scattering assay. *Eur. J. Biochem.* **214:**771–778
17. Chen, P.-Y., Pearce, D., Verkman, A.S. 1988. Membrane and water permeability determined quantitatively by self-quenching of an entrapped fluorophore. *Biochemistry* **27:**5713–5718
18. Cohen, B.E. 1986. Concentration- and time-dependence of amphotericin-B induced permeability changes across ergosterol-containing liposomes. *Biochim. Biophys. Acta* **857:**117–122
19. Dalla Serra, M., Menestrina, G. 1993. A fast-kinetic approach to the fluorimetric determination of the effects of membrane perturbing agents on lipid bilayers. *Life Sci. Adv. Biophys.* **12:**109–117
20. De Los Rios, V., Mancheno, J.M., Lanio, M.E., Onaderra, M., Gavilanes, J.G. 1998. Mechanism of the leakage induced on lipid model membranes by the hemolytic protein sticholysin II from the sea anemone *Stichodactyla helianthus. Eur. J. Biochem.* **252:**284–289
21. Garcia, A.M. 1986. Methodologies to study channel-mediated ion fluxes in membrane vesicles. *In*: Ionic channels in cells and model systems. R. Latorre, editor. pp. 127–140. Plenum Press, New York
22. Ginsburg, H., Stein, W.D. 1987. Biophysical analysis of novel transport pathways induced in red blood cell membranes. *J. Membrane Biol.* **96:**1–10
23. Inoue, T., Kamaya, H., Ueda, I. 1985. Stopped-flow study of anesthetic effect on water-transport kinetics through phospholipid membranes. Interfacial versus lipid core ligands. *Biochim. Biophys. Acta* **812:**393–401
24. Kem, W.R. 1988. Sea anemone toxin: Structure and action. *In*: The Biology of Nematocysts. D.A. Hessinger, H.M. Lenhoff, editors. pp. 375–405. Academic Press, San Diego
25. Kem, W.R., Dunn, B.M. 1988. Separation and characterization of four different amino acid sequence variants of a sea anemone (*Stichodactyla helianthus*) protein cytolysin. *Toxicon* **26:**997–1008
26. Kreitman, R.J., Pastan, I. 1998. Immunotoxins for targeted cancer therapy. *Adv. Drug Deliv. Rev.* **31:**53–88
27. Kuga, S. 1981. Pore size distribution analysis of gel substances by size exclusion chromatography. *J. Chromatog.* **206:**449–461
28. Lacy, D.B., Stevens, R.C. 1998. Unraveling the structures and modes of action of bacterial toxin. *Curr. Opin. Struct. Biol.* **8:**778–784
29. Lande, M.B., Donovan, J.M., Zeidel, M.L. 1995. The relationship between membrane fluidity and permeabilities to water, solutes, ammonia, and protons. *J. Gen. Physiol.* **106:**67–84
30. Lanio, M.E., Morera, V., Alvarez, C., Tejuca, M., Gomez, T., Pazos, I.F., Besada, V., Martinez, D., Huerta, V., Padron, G., Chavez, M.A. 2001. Purification and characterization of two hemolysins from *Stichodactyla helianthus. Toxicon* **39:**187–194
31. Lelkes, P.I. 1984. Methodological aspects dealing with stability measurements of liposomes in vitro using the carboxyfluorescein-assay. *In*: Targeted drug delivery and biological interaction. G. Gregoriadis, editor. pp. 225–246. CRC Press, Inc., Boca Raton, Florida, USA
32. Lesieur, C., Vécsey-Semjén, B., Abrami, L., Fivas, M., van der Goot, F.G. 1997. Membrane insertion: the strategies of toxins (Review). *Mol. Membrane Biol.* **14:**45–64
33. MacDonald, R.C., MacDonald, R.I., Menco, B.P.M., Takeshita, K., Subbarao, N.K., Hu, L. 1991. Small-volume extrusion apparatus for preparation of large unilamellar vesicles. *Biochim. Biophys. Acta* **1061:**297–303
34. Macek, P., Belmonte, G., Pederzolli, C., Menestrina, G. 1994. Mechanism of action of equinatoxin II, a cytolysin from the sea anemone *Actinia equina* L. belonging to the family of actinoporins. *Toxicology* **87:**205–227
35. Macek, P., Zecchini, M., Pederzolli, C., Dalla Serra, M., Menestrina, G. 1995. Intrinsic tryptophan fluorescence of equinatoxin II, a pore-forming polypeptide from the sea anemone *Actinia equina* L., monitors its interaction with lipid membranes. *Eur. J. Biochem.* **234:**329–335
36. MacGregor, II, R.D., Tobias, C.A. 1972. Molecular sieving of red cell membranes during gradual osmotic hemolysis. *J. Membrane Biol.* **10:**345–356
37. Malovrh, P., Barlic, A., Podlesek, Z., Menestrina, G., Macek, P., Anderluh, G. 2000. Structure/function studies of tryptophan mutants of equinatoxin II, a sea anemone pore-forming protein. *Biochem. J.* **346:**223–232
38. Martin-Benito, J., Gavilanes, F., De Los Rios, V., Mancheno, J.M., Fernandez, J.J., Gavilanes, J.G. 2000. Two-dimensional crystallization on lipid monolayers and three-dimensional structure of sticholysin II, a cytolysin from the sea anemone *Stichodactyla helianthus. Biophys. J.* **78:**3186–3194
39. Mayer, L.D., Hope, M.J., Cullis, P.R. 1986. Vesicles of variable size produced by a rapid extrusion procedure. *Biochim. Biophys. Acta* **858:**161–168
40. Menestrina, G., Cabiaux, V., Tejuca, M. 1999. Secondary structure of sea anemone cytolysins on soluble and membrane-bound form by infrared spectroscopy. *Biochem. Biophys. Res. Commun.* **254:**174–180
41. Merzlyak, P.G., Yuldasheva, L.N., Rodrigues, C.G., Carneiro, C.M.M., Krasilnikov, O.V., Bezrukov, S.M. 1999. Polymeric nonelectrolytes to probe pore geometry: Application to the alpha-toxin transmembrane channel. *Biophys. J.* **77:**3023–3033
42. Mui, B.-S., Cullis, P.R., Evans, E.A., Madden, T.D. 1993. Osmotic properties of large unilamellar vesicles prepared by extrusion. *Biophys. J.* **64:**443–453
43. Olbrich, K., Rawicz, W., Needham, D., Evans, E. 2000. Water permeability and mechanical strength of polyunsaturated lipid bilayers. *Biophys. J.* **79:**321–327
44. Orbach, E., Finkelstein, A. 1980. The nonelectrolyte permeability of planar lipid bilayer membranes. *J. Gen. Physiol.* **75:**427–436
45. Paula, S., Volkov, A.G., Van Hoek, A.N., Haines, T.H., Deamer, D.W. 1996. Permeation of protons, potassium ions, and small polar molecules through phospholipid bilayers as a function of membrane thickness. *Biophys. J.* **70:**339–348
46. Paula, S., Akeson, M. Deamer, D.W. 1999. Water transport by the bacterial channel alpha-hemolysin. *Biochim. Biophys. Acta* **1418:**117–126
47. Pederzolli, C., Belmonte, G., Dalla Serra, M., Macek, P., Menestrina, G. 1995. Biochemical and cytotoxic properties of conjugates of transferrin with equinatoxin II, a cytolysin from a sea anemone. *Bioconjugate Chem.* **6:**166–173.
48. Reid, C., Rand, R.P. 1997. Fit to osmotic pressure data. *Biophys. J.* **73:**1692–1694
49. Renkin, E.M. 1954. Filtration, diffusion, and molecular sieving through porous cellulose membranes. *J. Gen. Physiol.* **38:**225–243
50. Ruf, H., Georgalis, Y., Grell, H. 1989. Dynamic laser light scattering to determine size distributions of vesicles. *Methods Enzymol.* **172:**364–390
51. Sabirov, R.Z., Krasilnikov, O.V., Ternovsky, V.I., Merzlyak, P.G. 1993. Relation between ionic channel conductance and conductivity of media containing different nonelectrolytes. A novel method of pore size determination. *Gen. Physiol. Biophys.* **12:**95–111
52. Sausville, E.A. 1997. Targeted toxins. *In*: Encyclopedia of Cancer. J.R. Bertino, editor. pp. 1703–1714. Academic Press, New York
53. Schultz, S.G., Solomon, A.K. 1961. Determination of the effective

hydrodynamic radii of small molecules by viscometry. *J. Gen. Physiol.* **44:**1189–1199

54. Schwarz, G., Robert, C.H. 1990. Pore formation kinetics in membranes, determined from the release of marker molecules out of liposomes or cells. *Biophys. J.* **58:**577–583
55. Song, L., Hobaugh, M.R., Shustak, C., Cheley, S., Bayley, H., Gouaux, J.E. 1996. Structure of staphylococcal alpha-hemolysin, a heptameric transmembrane pore. *Science* **274:**1859–1866
56. Tejuca, M., Dalla Serra, M., Ferreras, M., Lanio, M.E., Menestrina, G. 1996. The mechanism of membrane permeabilization by sticholysin I, a cytolysin isolated from the venom of the sea anemone *Stichodactyla helianthus. Biochemistry* **35:**14947–14957
57. Tejuca, M., Anderluh, G., Macek, P., Alvarez, C., Lanio, M.E., Marcet, R., Torres, D., Sarracent, J., Dalla Serra, M., Menestrina, G. 1999. Antiparasite activity of sea anemone cytolysins on *Giardia duodenalis* and specific targeting with anti-*Giardia* antibodies. *Int. J. Parasitol.* **29:**489–498
58. Varanda, A., Finkelstein, A. 1980. Ion and non electrolyte permeability properties of channels formed in planar lipid bilayer membranes by the cytolytic toxin from the sea anemone, *Stoichactis helianthus. J. Membrane Biol.* **55:**203–211
59. Vodyanoy, I., Bezrukov, S.M., Parsegian, V.A. 1993. Probing alamethicin channels with water-soluble polymers. Size-modulated osmotic action. *Biophys. J.* **65:**2097–2105